



# Characteristics of force coefficients and energy transfer for vortex shedding modes of a square cylinder subjected to inline excitation

Hrisheekesh Krishnan<sup>a</sup>, Amit Agrawal<sup>b,\*</sup>, Atul Sharma<sup>b</sup>, Mark Thompson<sup>c</sup>, John Sheridan<sup>c</sup>

<sup>a</sup> IITB-Monash Research Academy, India

<sup>b</sup> Department of Mechanical Engineering, Indian Institute of Technology Bombay, Powai, Mumbai 400076, India

<sup>c</sup> Department of Mechanical Engineering, Monash University, 3800, Clayton, Australia

## ARTICLE INFO

### Article history:

Received 15 July 2017

Received in revised form 29 March 2018

Accepted 24 April 2018

Available online 24 May 2018

## ABSTRACT

The nature of the circulation regions around a bluff body in a cross flow can vary considerably from the normal von Kármán vortex-shedding mode when subjected to external excitations. The dynamics of the circulation regions around the bluff body has a direct impact on the force coefficients of the bluff body. In the present work, we correlate the spectral content and characteristics of the force coefficients of different vortex-shedding modes, observed for a square cylinder that is subjected to external excitation in the form of inline sinusoidal pulsation, to the near body vortical events. The strengths of various circulation regions around the bluff body and its location of formation are used to assess the impact of the vortical events on the force coefficient characteristics. In addition, the implication of relative timing of vortical events with respect to the inline excitation on the energy transfer is also discussed.

© 2018 Elsevier Ltd. All rights reserved.

## 1. Introduction and literature survey

The problem of a steady inflow past bluff bodies and the resulting von Kármán vortex-shedding mode and its various transitions has been extensively studied in the past due to the practical significance of the problem in engineering applications. The vortex-shedding modes can significantly vary from the von Kármán vortex-shedding mode when there is unsteadiness in the inflow. Evidently, the change in vortical structures near the body also significantly affects the loads on the body. The prediction of loads for such unsteady inflows is important in marine structures and bodies that are capable of undergoing vibration (Williamson and Govardhan, 2004).

Several authors have studied the problem of pure sinusoidal flow of the form  $U = u_f \sin(2\pi f_e t)$ , relative to the bluff body (Williamson, 1985; Tatsuno and Bearman, 1990). The problem is characterized by the amplitude and the frequency of the velocity pulsation. In dimensionless form the Keulegan–Carpenter number,  $KC = u_f / f_e D$ , defines the amplitude and the Stokes number,  $\beta = Re / KC = D^2 f_e / \nu$  the frequency, where  $u_f$  the maximum amplitude of the fluctuating velocity is,  $f_e$  is the externally imposed frequency,  $D$ , the diameter of the bluff body and,  $\nu$  is the kinematic viscosity of the fluid. Williamson (1985) visualized the vortex-shedding modes for the pure sinusoidal flow that is relative to the circular cylinder. He also correlated the force coefficients with the near-body vortical events. The  $KC$  was varied from 0 to 60 for visualization, and 0

\* Corresponding author.

E-mail address: [amit.agrawal@iitb.ac.in](mailto:amit.agrawal@iitb.ac.in) (A. Agrawal).

to 35 for force measurements. Even though the original problem is symmetric, the vortex shedding could be symmetric or asymmetric depending on the value of KC. For  $KC < 7$ , no major vortices are shed during a half cycle, whereas for  $KC > 7$  large vortices are shed. Further, for a low KC of  $< 1.5$ , no separation was observed and for  $1 < KC < 4$ , the flow was symmetrical. In  $4 < KC < 7$ , the attached vortices were found to be unequal in strength. Between  $7 < KC < 15$ , a single vortex is shed in each half cycle. The shed vortices pair up and convect at an angle to the flow direction, clearly indicating the asymmetrical nature of the shedding. Williamson (1985) observed that the direction can switch intermittently in a single experiment or change in different experiments depending on the initial conditions. As a result of the vortical events, the structure may experience a mean lift coefficient due to the asymmetric nature of vorticity formation. The interaction of generated vorticity at the cylinder wall in previous cycles with the cylinder wall is crucial to determining the vorticity generation at a given instant, indicating the nonlinear nature of vorticity production. For  $15 < KC < 24$ , pairs of vortices are generated in each half cycle. In the first half of the cycle, a pair of vortices is shed at an angle to the direction of the relative motion and, in the next half cycle, another pair of vortices is shed in the opposite direction. For  $24 < KC < 32$ , a three-pair regime was found and, for  $32 < KC < 40$ , a four-pair regime was found. Although Bearman et al. (1985) investigated sinusoidal flow that is relative to a square cylinder, no information regarding the vortex formation was given. Zheng and Dalton (1999) numerically studied the same problem for  $\beta = 213$  and  $1 < KC < 5$ . Symmetric vortex structures were observed in  $KC < 1$ . For  $KC = 3$ , the vorticity structures were still symmetric. However, the drag coefficient was found to be low. For  $KC = 5$ , the vortex structures around the body were clearly asymmetric and, hence, the lift coefficient was also found to be nonzero and asymmetric.

When a mean current is present in addition to the sinusoidal excitation, the dynamics near the bluff body can change considerably. Several authors have considered an inlet mean flow with sinusoidal pulsation that has the form,  $u = u_m + u_f \sin(2\pi f_e t)$  (Barbi et al., 1986; Armstrong et al., 1986; Konstantinidis et al. 2007; Zhou and Graham, 2000). The number of parameters in the problem increases to three from two due to the additional mean component. The choice of nondimensional parameters is no longer unique. Depending on whether the flow is current dominated or wave-dominated, several authors nondimensionalize the mean velocity as  $V_r = u_m/(f_e D)$ , which is referred to as reduced velocity, or alternatively, the velocity scale used for Reynolds number is the fluctuating velocity while the mean velocity is nondimensionalized with respect to the fluctuating velocity, to give a current ratio (Zhou and Graham, 2000). In the present study, the flow field is considered as the natural vortex shedding perturbed by a fluctuating velocity component. In the present work, the Reynolds number is defined as  $Re = u_m D/\nu$ , and the fluctuating part is nondimensionalized as  $A^* = u_f/(2\pi f_e D)$ . The amplitude ratio is related to the Keulegan–Carpenter number through  $A^* = 2\pi KC$ . The external frequency is nondimensionalized with the inherent natural vortex-shedding frequency that corresponds to  $Re$ , (if the natural vortex shedding caused because Reynolds number is above the critical limit) as  $f^* = f_e/f_n$ .

The added mean part of inlet excitation promotes the von Kármán vortex shedding, in which the vorticity of the opposite sign rolls up in an alternate part of a cycle in an antisymmetric manner; meanwhile, the fluctuating component promotes the shedding of vortices in a symmetric manner in one half of the cycle. The two modes can compete, resulting in chaotic vortex shedding (Srikanth et al., 2011; Ongoren and Rockwell, 1988). Considering that there are a great number of vortex-shedding modes, it is normal to classify the vortex-shedding mode according to the number of vortices that are shed in a complete cycle. An S mode denotes a single vortex shed per cycle, and P mode denotes a pair shed per cycle. Thus, the usual von Kármán vortex shedding is the 2S mode, which indicates that two single vortices of opposite sign complete one cycle. In the literature, several vortex-shedding modes are referred to as P, 2P, P + S, 2P + 2S and are identified in a variety of perturbations that are parallel and transverse to the mean flow. The classification mentioned above is mainly applicable to antisymmetric vortex-shedding modes. However, with inline excitations, vortex-shedding modes in which the timing of the formation of the vortices is symmetric with respect to the inline excitation can occur. In such cases, it is usual to add S as a prefix, followed by the number of pairs of vortices (in Roman numerals) that are shed in a cycle, in order to differentiate symmetric modes from the antisymmetric mode. In literature, S-I, S-II, and S-III modes are observed as symmetric modes. In addition to the change in the vortex arrangement, synchronization, or a vortex lock-in phenomenon, occurs when the frequency of the external pulsation influences the natural vortex-shedding frequency to make a rational ratio.

Zhou and Graham (2000) numerically investigated a wave-dominated flow over a circular cylinder. The current ratio, which was defined as  $B = u_m/u_f$ , was varied from 0 to 1 in steps of 0.25. The Keulegan–Carpenter number was varied from 0.2 to 26, and the Stokes parameter was kept constant at 200. For the current ratio  $B = 1$  and  $KC = 1$ , von Kármán vortex shedding was identified, while for  $KC = 2$ , a pair of symmetric vortices were shed per cycle. For  $KC = 3$ , symmetric shedding of a pair of symmetric vortex pairs was found, while at  $KC = 4$ , a pair of asymmetric vortex couples were shed in a cycle. Zhou and Graham (2000), also examined the relevance of the Morison equation to such problems.

However, no explicit information about the effect of vortical events on the force characteristics is available. Armstrong et al. (1986) studied the effect of inline pulsatile flow on circular, D-Section, and flat plate bodies. For all geometries, the synchronization was found to be around  $f_e/f_n = 2.0$ . However, no flow visualization was provided. Barbi et al. (1986) conducted experiments for a high  $Re \sim 40000$  flow over a circular cylinder. They found subharmonic synchronization around the regions of  $f_e/f_n = 1.0$  and  $f_e/f_n = 2.0$ . The amplitude ratio was kept constant at 0.2, and the frequency was varied. They found that there was a progressive decrease in the vortex-shedding frequency before the lock-in at both,  $f_e/f_n = 1.0$  and  $f_e/f_n = 2.0$  (see Leontini et al., 2011; Barbi et al., 1986 for further details). In addition to the usual von Kármán vortex-shedding frequency, Armstrong et al. observed asymmetric vortex shedding around  $f_e/f_n = 0.7$ , which is locked in as a harmonic of the excitation frequency. Konstantinidis et al., (2007) investigated the timing of vortex shedding across the lock-in range of  $f_e/f_n = 2.0$ , for a pulsatile flow at a high  $Re \sim 2150$  for a circular cylinder. The region in the parameter

space they investigated was characterized by two self-exciting branches that were separated by a region in which there was no self-excitation of the flow. They observed both, the 2S and 2P modes and reported that the change between the vortex-shedding modes was random. While both modes coexisted in  $f_e/f_n = 1.74$ , for  $f_e/f_n > 2.0$ , only the 2S mode existed. The timing of the vortex shedding, with respect to the inflow oscillation, was not changed by the mode of vortex shedding. The lack of excitation in the middle of the lock-in region was attributed to the timing of the shedding of the vortex during the forward stroke of the cylinder. In addition, they speculated about a possible phase jump near the first response branch and the hysteresis effects on either side. Konstantinidis and Balabani (2007) found symmetric vortex shedding at  $Re \sim 1200$  between  $f_e/f_n = 3$  and  $f_e/f_n = 4$ , with periodic flow forcing. They found that the symmetric vortex shedding breaks down into an antisymmetric mode downstream. In another experiment, Konstantinidis et al. (2007) observed bimodal vortex shedding in which the vortex-shedding mode changed from the 2S mode to the 2P mode in a single experiment. They observed this behavior in  $f_e/f_n < 2$  and inside the lock-in region. The 2P mode was not found for  $f_e/f_n > 2$ . Most of these studies were conducted for a current-dominated flow.

While the vortex-shedding modes observed in a current-dominated flow are documented in the literature, there is a scarcity of data available on the correlation of force coefficients associated with the near body vortical events. It is expected that the near-body vortical events will significantly impact the characteristics of the force coefficients. In addition to the force exerted, the phase of the dynamics of the near-body vortical region formation with respect to the inline excitation determines the energy transfer between the bluff body and the surrounding fluid. For example, Konstantinidis and Balabani (2007) associated symmetric vortex shedding with positive energy transfer to the cylinder on the basis of available information about the relative phasing of vortical events with respect to inline excitation.

Several of the vortex-shedding modes discussed in the present work have previously been observed by other authors in a variety of contexts, such as different bluff body geometries and methods of perturbation. Given that the vorticity dynamics are similar, some of the characteristics of the force coefficients could also be similar for such cases. The present work attempts to answer questions such as; Which vortical events are likely to be reflected in force coefficients for the canonical modes observed in the present study? How P mode generates mean lift? How is the slow frequency content of modulated wake and P mode reflected in the force coefficients? How the energy transfer between bluff body and fluid correlated with the near body vortical events?

To clarify such questions, we characterize the circulation strengths and location of formation of various vortical structures of several canonical vortex shedding modes. By using timed snapshots of vorticity contour, the frequency content and its correlation with the vortical events and the wake structure are explicitly examined. The timed snapshots are also used to assess the impact of timing of vortical events with respect to the inline excitation, on the energy transfer between bluff body and fluid. Note that vorticity generation and its transport around the bluff body to form different circulation regions and how these circulation regions convect around the bluff body are all important in the correlation of force coefficients with respect to the vorticity dynamics. Due to the similarity in vorticity dynamics, the characteristics of force coefficients could be similar across different bluff bodies and flow parameters, for a given vortex shedding mode. However, this characteristic similarity between modes of similar nature arising under different conditions is expected to be only qualitative.

## 2. Problem description and computational details

In the present study, inline excitation is provided by employing velocity of the formula  $u = u_m + u_f \sin(2\pi f_e t)$  and  $v = 0$  at the inlet, and on the lateral sides. At the outlet, the convective boundary condition is employed. Flow is initially assumed to be at rest. The Reynolds number is computed based on the mean flow and is kept constant at  $Re = 100$ . The nondimensional frequency ratio was varied from 0.6 to 1.4 in step of 0.1, and the amplitude ratio was varied from 0.1 to 0.6 in step of 0.1. The flow domain along with the initial and boundary conditions employed in the simulation is given in Fig. 1. The domain size was chosen to be 15D at the inlet and on the lateral sides. The outlet is kept at 55D from the square cylinder rear side.

The evolution of flow variables is computed using D2Q9 Lattice Boltzmann Method with a single relaxation time and Bhatnagar–Gross–Crook operator (see Succi, 2001 for more details). For a given Reynolds number, we chose a mean flow speed and then specify the dimension of the bluff body in lattice units. Then the viscosity of the fluid is set to match the given Reynolds number. The evolution of flow field is computed in the following manner: the particle distribution function at each node is initialized to the equilibrium value corresponding to the initial values of the flow variables. The evolution of particle distribution functions is tracked by lattice propagation step given in Eq. (2) and collision step given in Eq. (3)

$$f_i(\vec{x} + \vec{e}_i, t + \delta_t) = f_i^n(\vec{x}, t) \quad (1)$$

$$f_i^n(\vec{x}, t) = f_i(\vec{x}, t) - (f_i(\vec{x}, t) - f_i^{eq}(\vec{x}, t))/\tau \quad (2)$$

where  $f_i^n(\vec{x}, t)$  and  $f_i^{eq}$  are the post-collision distribution function and equilibrium density function at a node. The latter function is computed as:

$$f_i^{eq}(\vec{x}, t) = \rho w_i \left( 1 + 3(\vec{e}_i \cdot \vec{u}) + \frac{9}{2}(\vec{e}_i \cdot \vec{u})^2 - \frac{3}{2}(\vec{u} \cdot \vec{u}) \right) \quad (3)$$

where  $\rho$  denotes the macroscopic density at the node;  $\vec{u}$  denotes the macroscopic velocity vector;  $\vec{e}_i$  denotes the lattice vectors of the D2Q9 scheme; and  $w_i$  denote the lattice constants for each lattice vector. At the boundaries, the equilibrium

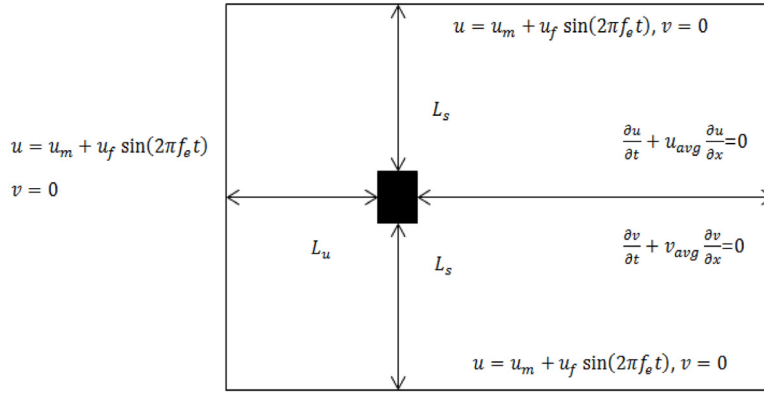


Fig. 1. Initial and boundary conditions for flow past the square cylinder that is subjected to inline pulsation. Domain size,  $L_u = 15D$ ,  $L_d = 55D$ ,  $L_s = 15D$ .

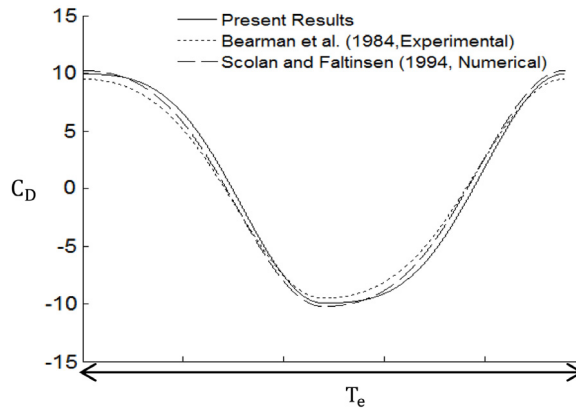


Fig. 2. Comparison of drag coefficient for  $\beta = 213$  and  $KC = 3$  with literature.

distribution functions are computed after the collision step, from the known value of macroscopic variables and propagated to the next step. On the wall, the no slip boundary condition is implemented using the bounce back scheme.

At each time step, the macroscopic variables are recovered from the known distribution functions by using Eq. (4).

$$\rho = \sum_{i=0-8} f_i, \quad \rho \vec{u} = \sum_{i=0-8} f_i \vec{e}_i, \quad p = \rho C^2 \tag{4}$$

where  $p$  denotes the macroscopic pressure, and  $C$  is the lattice speed of sound for the D2Q9 scheme.

The present code has been validated extensively for steady inflow problem by Kumar et al. (2008) and unsteady oscillation problems by Sewatkar et al. (2012). Detailed grid independence study for the problem is given by Krishnan et al. (2016). Further, we calculate the inline force that acts on the square cylinder that is purely under oscillatory flow conditions, for  $\beta = 213$  and  $KC = 3$ . A grid resolution of 32 grid points per side of the square cylinder was used for both the benchmark cases. The calculated drag coefficient is compared with the experimental results of Bearman et al. (1985) and the numerical results of Scolan and Faltinsen (1994), in Fig. 2. The drag coefficient of the experimental and numerical results is computed using the given coefficients of Morison’s equation by Bearman et al. (1985) and Scolan and Faltinsen (1994) in their respective works. The drag coefficient that was computed matches well with these experimental and numerical results.

### 3. Results and discussion

The effect of non-dimensional amplitude and frequency of the inline pulsatile free-stream flow, on the instantaneous, mean, and r.m.s. value of force (lift and drag) coefficients as well as energy transfer between the fluid-flow and the square-cylinder, is presented below at a constant Reynolds number  $Re = 100$ . Other non-dimensional governing parameters are varied as follows:

- Amplitude ratio,  $A^* = 0.1$  to  $0.6$  in step of  $0.1$
- Frequency ratio,  $f_e/f_n = 0.6$  to  $1.4$  in step of  $0.1$ .

The results are presented separately for the various vortex-shedding modes – correlating the vortical structures with the force coefficients in each flow-regime.

In our recent work (Krishnan et al. 2016), a flow regime map was prepared for the above parametric study, shown in Fig. 3. Furthermore, in the earlier work, we demonstrated a good match between our regime map and the vortex-shedding modes (for square-cylinder) with that for the inline acoustic excitation experiments for the circular cylinder (Detemple-Laake and Eckelmann, 1989). Due to the weakly compressible nature of the flow, it was considered more appropriate to compare the present results with acoustic experiments. Finally, a detailed discussion on the formation of various vortex-shedding modes was also presented. Because this work depends on the results of the earlier work, particularly based on the proposition that the vorticity-dynamics in the various vortex-shedding modes relate to their effect on the force-coefficients, a brief summary of the salient results is given in the following paragraphs.

The regime map in Fig. 3 shows that the parametric-space (oscillation frequency versus amplitude) is subdivided into six different regions – corresponding to five flow regimes or modes of vortex-shedding: 2S, 2P + 2S, modulated-wake or beating-string, P, and Symmetric. With increasing amplitude at various  $f_e/f_n$ , the flow regime map shows four transitions in vortex-shedding modes: first, the 2S → 2P + 2S mode at  $f_e/f_n = 0.6$  (under sub-harmonic synchronization); second, 2S → modulated wake mode (no synchronization) for  $f_e/f_n = 0.7, 0.8$ , and  $f_e/f_n \geq 1.2$ ; third, 2S → P → Symmetric mode (under harmonic synchronization) for  $f_e/f_n = 0.9$  and 1.0; and fourth, the 2S → modulated-wake → Symmetric mode at  $f_e/f_n = 1.1$ .

With increasing amplitude, the figure shows that all the four transitions from the 2S mode occur at  $A^* = 0.3$ , for all  $f_e/f_n$ ; the third and fourth transitions – to P-Symmetric mode – occur at  $A^* = 0.5$  for the intermediate range of  $f_e/f_n$ . During the modulated wake or beating string mode, the direction of vortex shedding alternates over a few vortex shedding cycles; and there is no synchronization between the two types of periodic flow – natural vortex shedding flow and the external oscillation of incoming flow. The synchronization is sub-harmonic in the 2P + 2S mode and harmonic in the P-mode of flow regime. The pair of shed-vortices is symmetric about the horizontal centerline in the Symmetric mode, as discussed below.

The dynamics of vortical formation leaves a trace in the spectra of lift coefficient of each vortex-shedding mode. The typical spectral characteristics of various vortex shedding modes observed are shown in Fig. 4. The spectra of the lift coefficient of the 2P + 2S mode show a major peak at half the imposed frequency (P1) in Fig. 4(a), indicating subharmonic synchronization. The modulated wake mode shows three peaks P1, P2 & P3. These three major components of spectra can be understood as an amplitude modulation process between natural vortex shedding frequency and the imposed frequency (see Leontini et al., 2011). The spectra of the P-mode (Fig. 4(d)) show a peak at the imposed frequency (P2 in Fig. 4(c)), which indicates harmonic synchronization, although the maximum peak is observed at zero frequency (P1 in Fig. 4(c)) due to the asymmetric vortex shedding. The spectra of the Symmetric mode show rather broadband spectra with no peaks. The mean lift coefficient is reduced to almost zero due to the symmetric nature of the vortex shedding. However, the visualization of vortex shedding over a cycle confirms that symmetric vortex shedding is under harmonic synchronization (see Krishnan et al., 2016).

### 3.1. Correlation of force coefficients with near-body vortical events

In this section, over a single/multiple time period of inline pulsation/natural vortex shedding, we discuss the temporal variation of force coefficients for the various vortex-shedding modes. The near-body vortical events will leave a trail on the force characteristics of each vortex shedding mode, due to the circulation regions formed/present around the body at different locations and its evolution over time.

Any phase difference between the incoming flow and the forces acting on the bluff body must be due to the second term and by understanding the relative timing of various vortical events one can obtain meaningful results on the nature of energy transfer between bluff body and fluid flow. The objective is to correlate the near-body vortical events to the major frequency components of the force coefficients and to also understand the effect of relative phasing of vortical events on the energy transfer. In Fig. 5, the alphabetical order from (a) to (e) indicates the instantaneous value of sinusoidal pulsation over a cycle. In all the subsequent force-coefficient plots, the timing is shown with reference to Fig. 5, unless mentioned explicitly otherwise.

#### 3.1.1. 2P + 2S vortex-shedding mode

First, we examine the 2P + 2S mode, which is observed at the lowest frequency ratio studied here. Since this flow is under subharmonic lock-in, two cycles of inline pulsation complete the 2P + 2S mode. Hence, in Fig. 6(f, g), the temporal variation of the lift and drag coefficient is shown over two cycles of external pulsation time period for  $Re = 100$ ,  $f_e/f_n = 0.6$ , and  $A^* = 0.4$ . It can be verified from the figure that the temporal variation over the second cycle is a mirror image (with respect to the horizontal line) of the first cycle for the lift coefficient, and the drag coefficients are almost the same. In the first half of the first cycle, one-pair of vortices (P) is shed and one-single vortex (S) is shed, while in the second half, one P is shed in the opposite direction and one S is shed, totaling to 2P + 2S over two cycles of incoming excitation.

At the start of the cycle, Fig. 6(a) shows that a pair of vortices is convected into the wake toward the upside, which was formed in the previous cycle; thereafter, Fig. 6(b) shows that this pair of vertices has been completely shed into the wake. During this process, the lift coefficient has reached a local minimum close to point (b) due to the proximity of the oppositely signed shear layer for a brief period (the red lower region in Fig. 6(b)); however, the drag coefficient ((b) to (c) in Fig. 6(g))

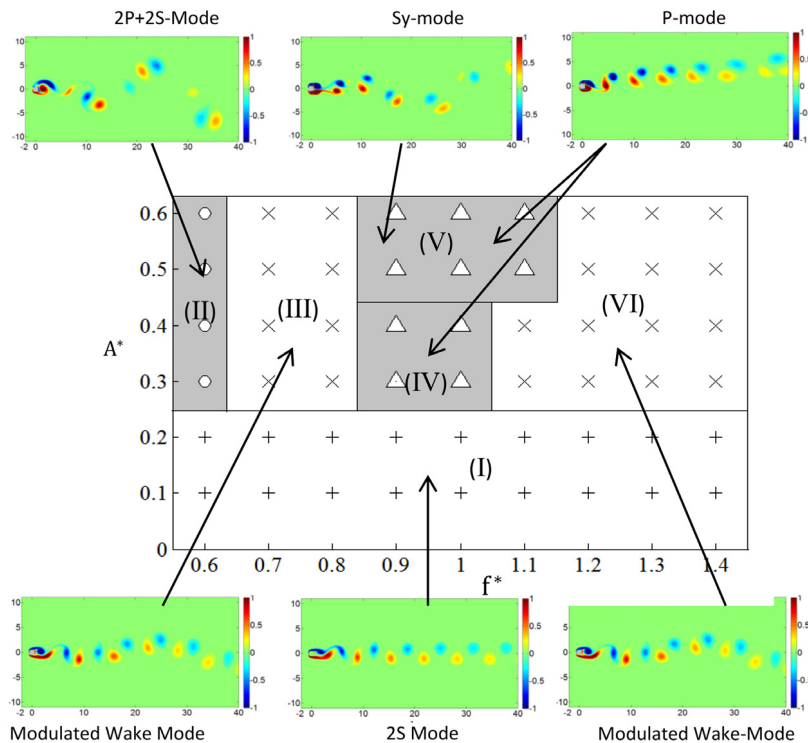


**Fig. 3.** Flow regime map of a square cylinder subjected to inline pulsation at  $Re = 100$ , Present results (I) 2S mode; (II) 2P + 2S mode, subharmonic synchronization; (III) Beating String mode; (IV) P Mode, harmonic synchronization; (V) Symmetric mode and P-mode; and (VI) Beating String mode. The transitions between the regions are known only within the resolution of the parameters investigated. The transitions between the various regions may not be straight lines as indicated. Vorticity contours, in the various regimes, are also shown. Gray regions indicate lock in regions. Source: Adapted from Krishnan et al. 2016.

falls rapidly just after the departure of the P vortex pair. From Fig. 6(c) to (e), it can be observed that a pair of vortices is being formed of the opposite sign when compared to the first half of the cycle. It should be noted that a single (clockwise) vortex is also shed in between Fig. 6(c) and (e) as a tail-end shear layer process. The effect of formation of a vortex-pair (P) in the downward direction, during (c)–(d)–(e), is to cause a positive lift coefficient, while increasing the drag that acts on the body.

To assess the impact of various circulation regions on the force coefficients, the relative strengths of various circulation regions and the positions of vorticity extrema are calculated by isolating each of these vortex structures in the computational domain. The extent of circulation regions is determined by incorporating all vorticity contour levels greater than 0.1% of the global maxima of the peak vorticity. The circulation is calculated by evaluating the integral  $\Gamma_n = \iint \omega dA$  over isolated vortical regions; the local extrema are found using a local neighbor search algorithm (Kumar et al., 2008). A wider snapshot of the vorticity contour of 2P + 2S mode in Fig. 6(d)) is shown in Fig. 7; at the time-instant corresponding to the maximum lift-coefficient. At this time instant, Fig. 7 clearly shows the various types of vortical structures (S for Single and P for Pair of shed-vortices; and B for Base-region and S for Shear-layer attached-vortices) that evolve during the formation of 2P + 2S mode. If a vortical structure is part of a pair in 2P + 2S, it is indicated as P, followed by the first letter of the sign (P for Positive and N for Negative) of the vortical structure, and the location of already shed vortices for previous cycles are indicated by the number. The number suffixes indicate that the vortices are shed one cycle before the presented snapshot. The capital letter B indicates that the vortical region originates in the base region, and SP and SN denote positive and negative shear layers, respectively while BP represents base region positive vorticity and BN represents base region negative vorticity. SN1 refers to the single vortex shed into the wake in 2P + 2S mode and PP1 and PN1 denote the pair of vorticity region, with positive and negative vorticity respectively. The X and Y coordinates are shown in brackets in Fig. 7, near to each vertical structure. The value shown in dashed box is the circulation strength and the value shown in solid box is peak vorticity.

The strengths of the computed circulation regions are nondimensionalized by dividing the circulation strength with  $U_m D$ , and is given in Table 1. The positive vortex maxima are shown in white circles, while the negative minima are shown with a plus sign; furthermore, the strength is nondimensionalized by dividing the vortical value with  $U_m/D$ . The coordinates of various maxima and minima are given with reference to the coordinate system with the origin at the center of the square cylinder. A positive value of the Y coordinate of the vortex center implies that the point is above the wake center line, while the negative value implies that the vortex center is below the wake center line.

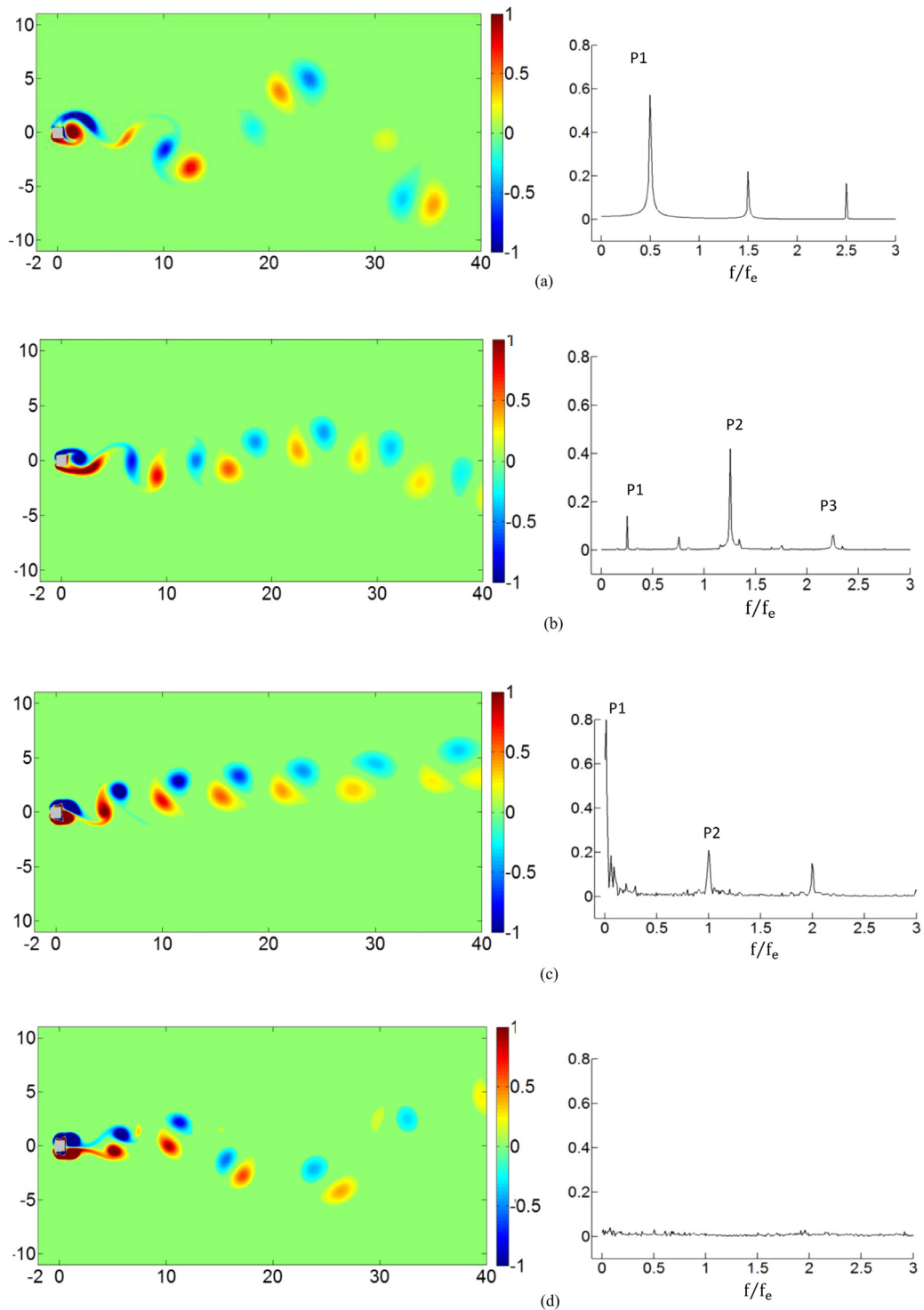


**Fig. 4.** Vorticity contours and spectra at the various vortex shedding modes at  $Re = 100$ : (a) 2P + 2S mode (shedding with half the imposed frequency), at  $A^* = 0.4$ ,  $f_e/f_n = 0.6$ ; (b) Modulated-wake mode, at  $A^* = 0.4$ ,  $f_e/f_n = 0.8$ ; (c) P-mode (shedding with the imposed frequency), at  $A^* = 0.4$ ,  $f_e/f_n = 0.9$ ; and (d) Symmetric mode, at  $A^* = 0.6$ ,  $f_e/f_n = 0.9$ .

From Table 1 and Fig. 7, it can be inferred that the closest vortical structures to the body are the base region vortical regions and the shear layers. The rolling up of the negative shear layer (SN) has the maximum impact on the lift coefficient,

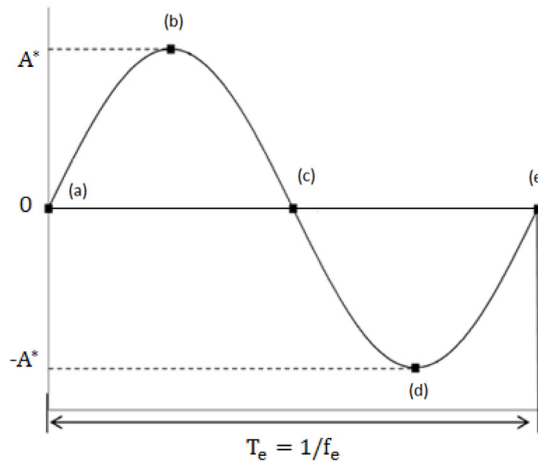


Fig. 5. Timing of inline pulsation over a cycle indicated from (a) to (e).

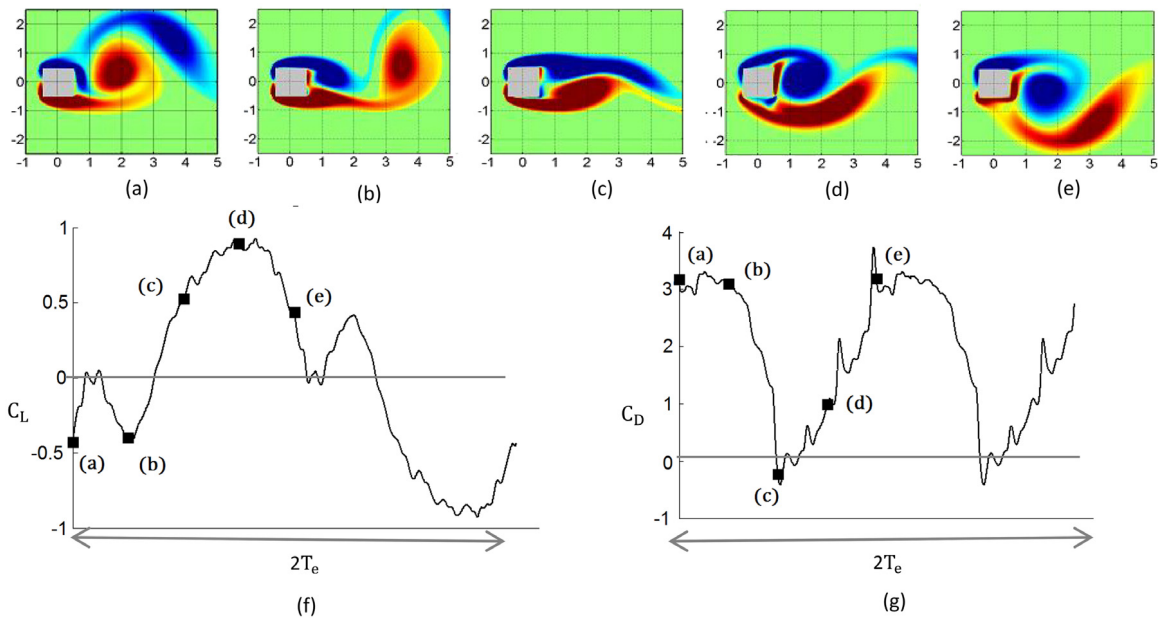
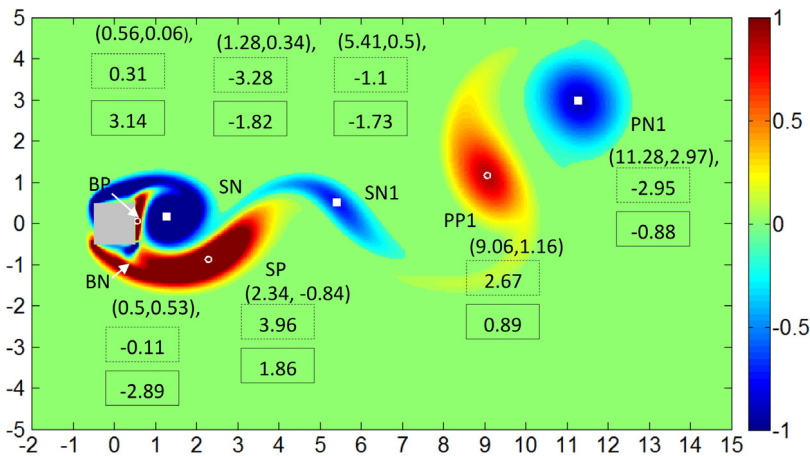


Fig. 6. Temporal variation of (a)–(e) vorticity-contours, and (f)–(g) lift and drag coefficient, over two time period of external pulsation ( $2T_e$ ) for  $2P + 2S$  mode at  $Re = 100$ ,  $f_e/f_n = 0.6$   $A^* = 0.4$ . The frame-size considered for the contour plots in (a)–(e) is  $5D \times 6D$ . (For interpretation of the references to color in this figure legend, the reader is referred to the web version of this article.)

which is both due to the proximity to the body and to the strength of the circulation region. The single vortex that is formed in the  $2P + 2S$  mode is at a distance of  $5.4D$  from the wake center and, hence, unlikely to have any impact on the force coefficients. The entire process of P formation happens in the latter part of the cycle.

It is informative to compare the vortical structures of  $2P + 2S$  mode to the vortex shedding without any excitation. The vortical structures for vortex shedding without excitation are evaluated when the lift coefficient is at its maximum, which is shown in Fig. 8. The strengths of the circulation regions given in Fig. 8. Compared to the  $2P + 2S$  mode, the strengths of the circulation regions are weaker. The strength of the base region vorticity is negligible, and the roll-up of the negative shear layer occurs approximately  $0.66D$  away from the base region when compared to the  $2P + 2S$  mode. Thus, the stronger vortical regions that is nearer to the body cause higher base region vorticity and also higher force coefficients. The difference in the absolute strength of the circulation between the vortices in the P vortex pair is not appreciable. A pair of vortices tends to form simultaneously in the P formation.



**Fig. 7.** Vortical structures near the body for at maximum lift coefficient shown as (d) in Fig. 6 for 2P + 2S mode, for  $Re = 100$ ,  $f_e/f_n = 0.6 A^* = 0.4$ . X and Y coordinates are shown in brackets. Value shown in dashed box is the circulation strength and value shown in solid box is peak vorticity. For description and value of circulation regions refer Table 1.

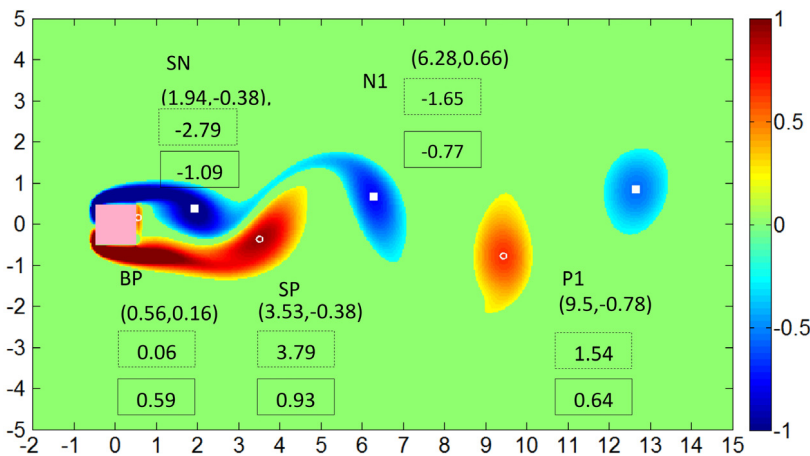


**Fig. 8.** Vortical structures near the body at the maximum lift coefficient shown for vortex shedding without excitation at the maximum of the lift coefficient that is at  $Re = 100$ .

**Table 1**  
Strength and positions of the various circulation regions that are shown in Fig. 7, 2P + 2S mode.

Region	Description	Circulation strength (Nondimensionalized)	Position of vortex center from center of square cylinder		Local maxima/minima vorticity value (Nondimensionalized)
			X/D	Y/D	
BP	Base region vorticity, Positive	0.31	0.56	0.06	3.14
BN	Base region vorticity, Negative	-0.11	0.5	0.53	-2.89
SN	Shear layer, Negative vorticity	-3.28	1.28	0.16	-1.82
SP	Shear Layer, Positive vorticity	3.96	2.34	-0.84	1.86
SN1	Single vorticity region, Negative, Shed in present cycle	-1.11	5.41	0.5	-0.75
PN1	Vortex pair, Negative vorticity, Shed in the previous half cycle	-2.67	9.06	1.16	0.89
PP1	Vortex pair, Positive vorticity, Shed in the previous half cycle	2.5	11.28	2.97	-0.88

3.1.2. Modulated-wake vortex-shedding mode

Next, we examine the modulated wake that is observed at  $f_e/f_n = 0.7$  and  $f_e/f_n = 0.8$ . At these frequency ratios, the flow is not synchronized to the external excitation. The spectra shown in Fig. 4(b) contain three major components. The

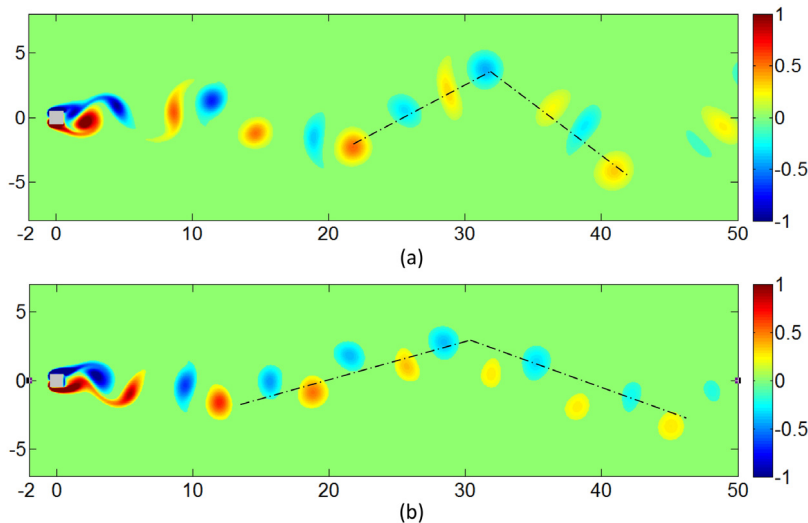


**Fig. 9.** Instantaneous snapshot of the modulated wake at  $Re = 100$  and  $A^* = 0.4$ : (a)  $f_e/f_n = 0.7$  and (b)  $f_e/f_n = 0.8$ ,  $A^* = 0.4$ ; the dash-dot lines contain approximately 6 vortices in (a) and 10 vortices in (b), within a complete swing of the wake.

maximum peak shown as P2 is the natural vortex-shedding frequency and is unaltered. This observation is different from the observations by Leontini et al. (2011), Smith et al. (2012) who observe a reduction in the natural frequency around this region. The present results are more similar to the acoustical experiment results of Detemple-Laake and Eckelmann (1989). The next peak, P1, is given as  $f_n - f_e$ . This frequency is slower than the natural vortex-shedding frequency. This P1 frequency arises because of the modulation of the basic natural vortex shedding by the imposed excitation.

The instantaneous snapshot of the vortex shedding in the modulated wake at  $f_e/f_n = 0.7$  and  $f_e/f_n = 0.8$  for  $A^* = 0.4$  is given in Fig. 9. An evident feature in Fig. 9 is the wake swinging, which is indicated by the dashed lines. It can be observed that this swinging is a phenomenon of slower frequency. It is possible to ascertain whether this corresponds to the slower frequency that is part of the spectra of the modulated wake that is shown in Fig. 4(b). The peak frequency, P2, is the natural vortex-shedding frequency; therefore, two vortices of opposite sign are shed in a cycle. For  $f_e/f_n = 0.7$ , the ratio of P2/P1 is approximately 3.3. This implies that the periodic phenomenon contains approximately 6.6 vortices. This can be confirmed by the number of vortices in the dashed line that is shown in Fig. 9(a). Similarly, for  $f_e/f_n = 0.8$ , the ratio of P2/P1 is 5, which implies that the periodic phenomenon contains 10 vortices. This is evident from Fig. 9(b).

The lift and drag coefficients for the modulated wake are given in Fig. 10(b) and (c). The frequency of the drag coefficient shown in Fig. 10(b) is the imposed external frequency. In order to further confirm the swinging of the wake, successive snapshots are shown in Fig. 10(a). The timing of the snapshots is given in Fig. 10(b). The snapshots correspond to the local extrema in lift coefficient. Fig. 10 shows that snapshots which are three frames apart (such as I & IV, and II and V) are almost mirror symmetric, that is they correspond to approximately 1.5 vortex-shedding cycles. The slower wake swinging is completed at the vortex-shedding cycle of approximately 3.3.

### 3.1.3. P vortex-shedding mode

Next, we examine the P vortex-shedding mode that is observed under harmonic synchronization for the square cylinder. The extensive study by Leontini et al. (2013) for circular cylinder also shows similar P mode around similar flow parameters and associate the same with a mean lift. In the present study, the spectra of the P mode show a peak at the zero frequency due to the mean lift coefficient, which is indicated as P2 in Fig. 4(c). The main frequency P1 shows the timing of the vortex formation pair. However, unlike the natural vortex shedding, the pair of vortices tends to form together in a part of the cycle. The temporal variation of the lift and drag coefficient over two cycles in the P mode at  $Re = 100$ ,  $f_e/f_n = 0.4$  and  $A^* = 0.4$  is shown in Fig. 11. The vortical structure corresponding to the peak of the lift coefficient can be seen in Fig. 11(c); zoomed-out view shown in Fig. 12. At this instant, one can observe that a pair of vortices is being formed closer to the bluff body in the wake as compared to similar vortical structures of natural vortex shedding. It is the rolling up of the positive shear layer that is nearer to the body, the main vortical event that causes the peak that is observed in the lift coefficient. During the formation of P, the drag also increases. During the brief period when the negative shear layer is in close contact with the body, shown as (d)–(e) in Fig. 12, there is a positive peak in lift coefficient. Thus, the asymmetry in the lift coefficient is not only due to the differing circulation strength but also due to the differing amounts of time for which each shear layer is in contact with the body. The P formation resembles the vortical processes that are similar to the P formation in the 2P + 2S mode; however, the direction of vortex shedding does not alternate in the case of the P mode. Furthermore, the phase of the pair vortex formation shifts to the former part of the cycle in comparison to the vortex formation of the 2P + 2S mode.

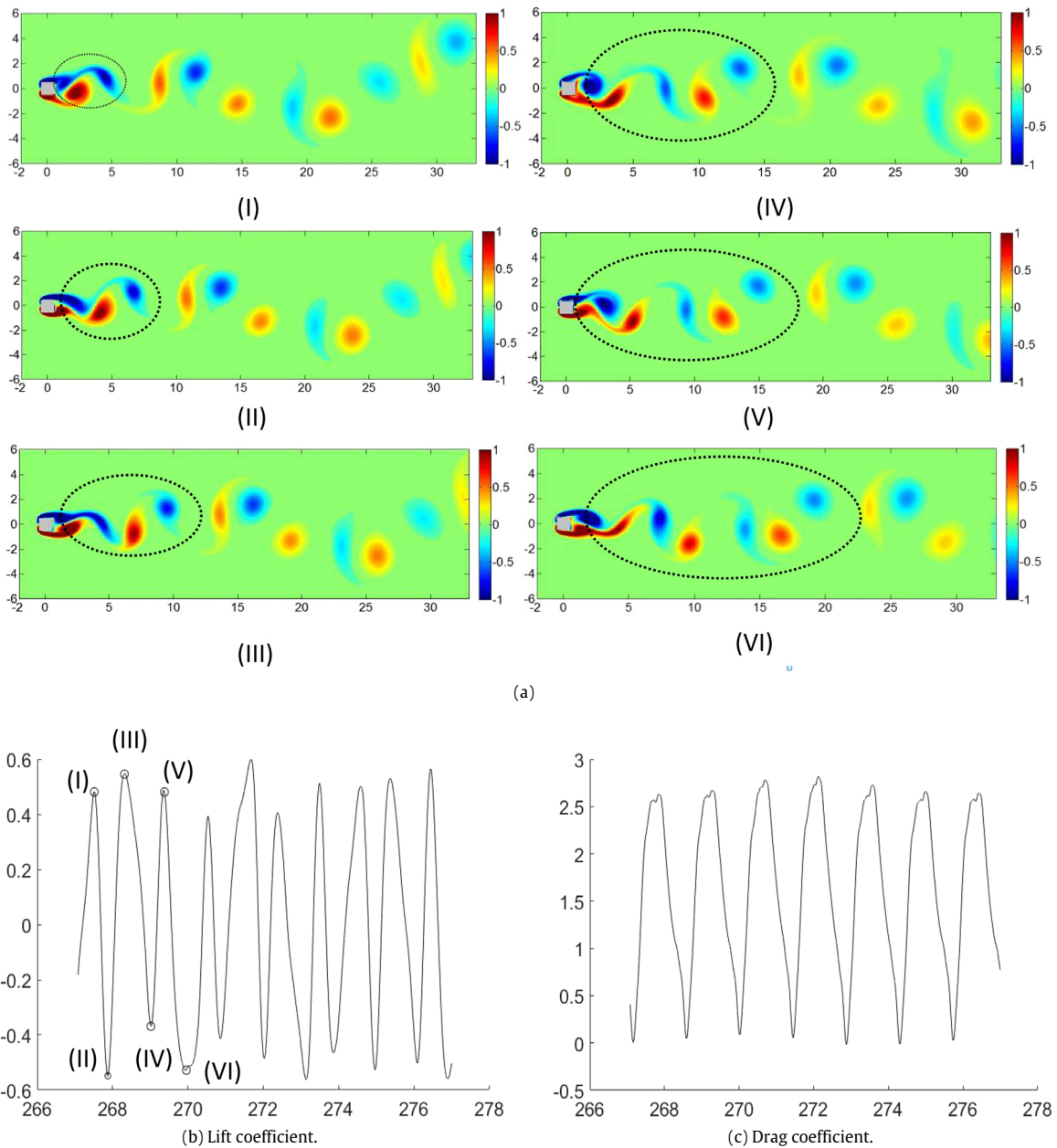


**Fig. 10.** (a) Temporal variation of instantaneous vorticity contours in the modulated wake mode for  $Re = 100$ ,  $f_c/f_n = 0.7$ , and  $A^* = 0.4$ . Time instants corresponding to the contours in (a) is given in Fig. 10(b). The encircled region in (a) shows the successive shedding of vortices. Swinging of the wake phenomenon is evident. The wake swinging is given by the P1 frequency content shown in Fig. 4(b).

### 3.1.4. Symmetric vortex-shedding mode

The symmetric mode observed at the left lock-in boundary of the harmonic synchronization region is now examined. The spectra of the lift coefficient are broadband, as shown in Fig. 4(d). This is due to the approximately symmetric vortical generation and the interaction around the body. The lift coefficient shows random fluctuations around the mean as shown in Fig. 13. In a perfectly symmetric mode such as the S-II mode, the lift coefficient is exactly zero, and the base region vortices couple with the shear layer vortices, yielding two pairs of vortices. Xu et al. (2006) distinguish between the approximate symmetric mode as S-I mode while the perfectly symmetric mode is described as S-II mode. In literature often the distinction is not made between the two types of symmetric modes and it is usual to refer both modes as symmetric mode. In the case of the presently observed approximately symmetric mode, the strengths and positions of the vortical regions vary slightly from cycle to cycle, and the wake length is stochastic. Konstantinidis and Balabani (2007) observed

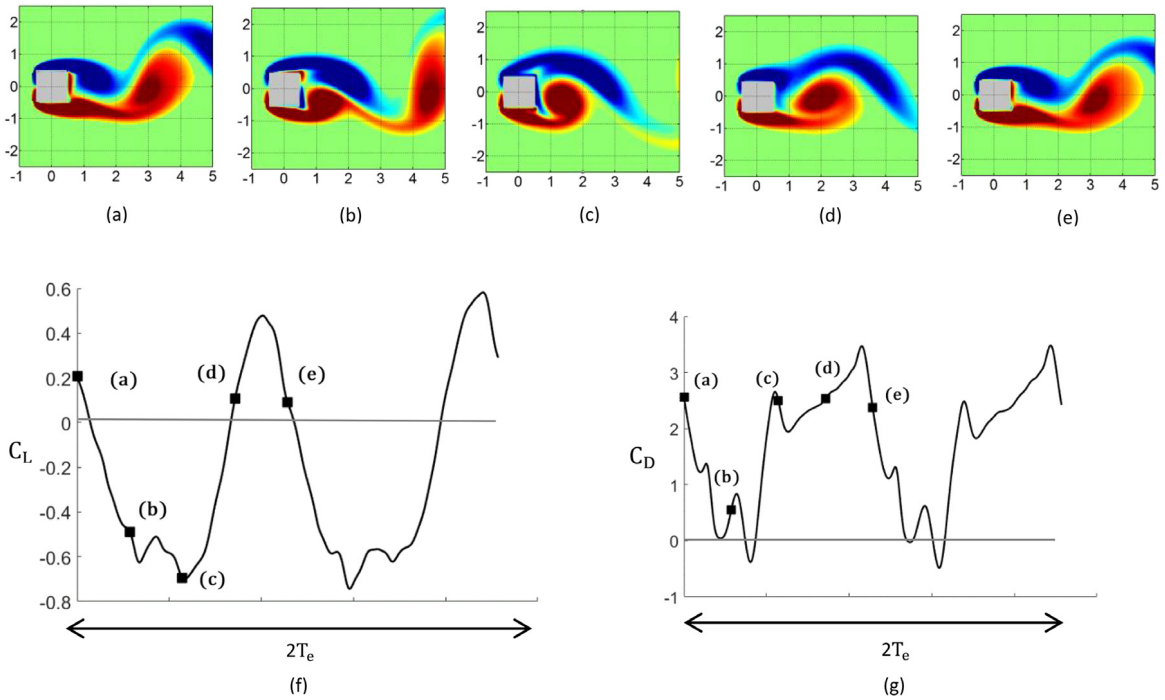


**Fig. 11.** Temporal variation of (a)–(e) vorticity-contours, and (f), (g) lift and drag coefficient, for P mode,  $Re = 100, f_e/f_n = 1.0, A^* = 0.4$ .

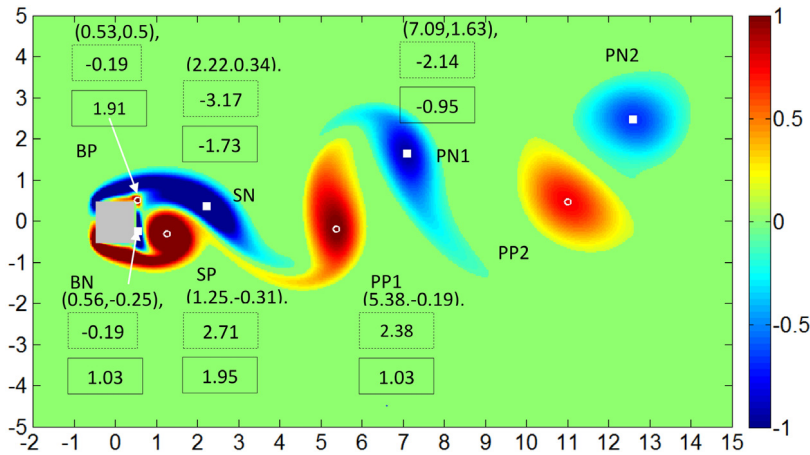


**Fig. 12.** Vortical structures near the body for at maximum lift coefficient for P mode shown as (c) in Fig. 11.

similar approximately symmetric vortex-shedding mode in their experiments. Al-Mdallal et al. (2007) also observed similar approximately symmetric vortex shedding for circular cylinders in their numerical simulations and they found the mean and RMS value of lift coefficient was close to zero, though not exactly zero. This confirms the similarity in the force coefficients over a wide range of Reynolds number and bluff bodies. Various vortical regions are indicated in Fig. 14. The positions and the strengths of the circulation regions are only approximately symmetric, including the base region vortices. The pair formation shifts completely to the first part of the cycles, and the drag coefficient also increases during the pair formation.

### 3.2. Long-term averages of lift and drag coefficients

This section focuses on the mean and RMS values of the lift and drag coefficients. In all cases, the values were obtained by taking sample data for 60 cycles of natural vortex-shedding. The values of  $C_{D,mean}$ ,  $C_{D,rms}$ ,  $C_{L,mean}$ , and  $C_{L,rms}$  for various frequencies and amplitudes are given in Fig. 15(a), (b), (c), and (d), respectively. The frequency resolution of the data around

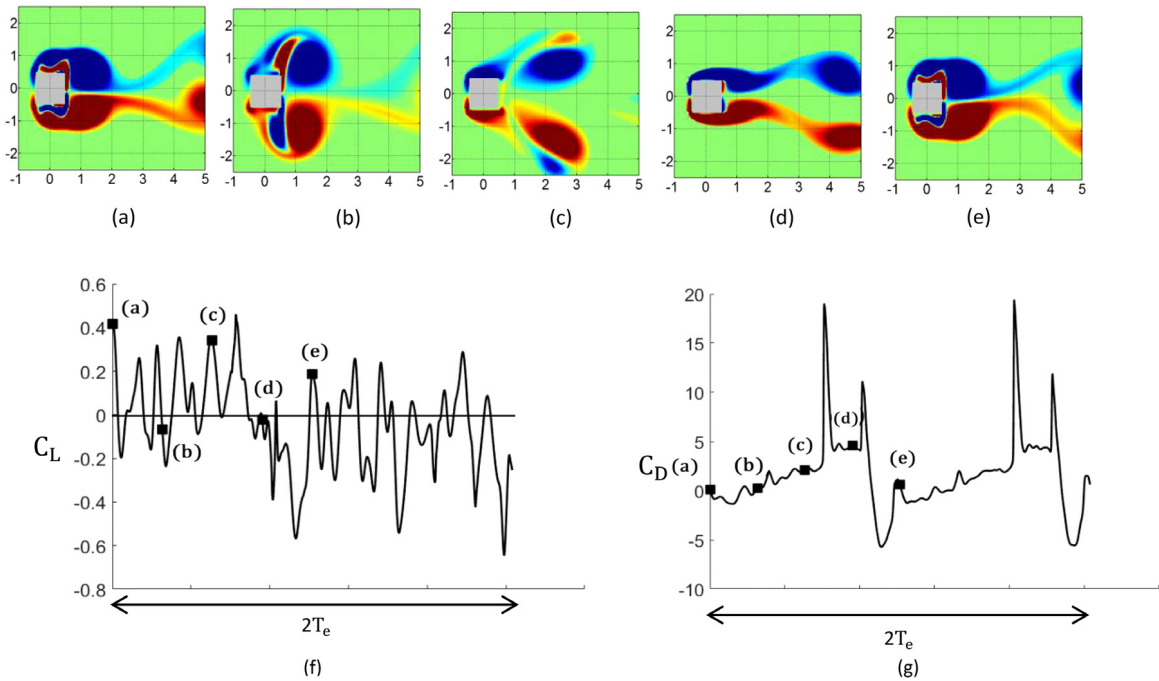


Fig. 13. Temporal variation of (a)–(e) vorticity-contours, and (f)–(g) lift and drag coefficient, Lift and drag coefficient over two time period of external pulsation ( $2T_e$ ) for Symmetric mode,  $Re = 100, f_e/f_n = 0.9, A^* = 0.5$ .

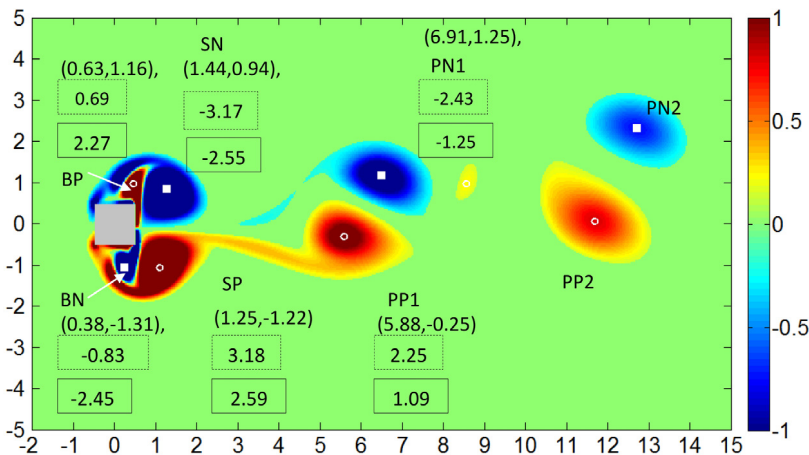


Fig. 14. Vortical structures near the body for Symmetric mode at time instant (b) in Fig. 13.

the fundamental synchronization region was increased by carrying additional simulations at  $f_e/f_n = 0.85, 0.95 \& 1.05$ , in addition to the simulations carried out in Section 3. For the force curves, the results of amplitudes greater than 0.2 are only plotted. For  $0.6 \leq f_e/f_n \leq 0.8$ ,  $C_{D,mean}, C_{D,rms}$ , and  $C_{L,rms}$  values decrease with an increase in the driving frequency for a given amplitude. As the amplitude of the inline excitation is increased while keeping the frequency ratio constant, the values of the various average and RMS force parameters increases. The  $C_{L,mean}$  values are negligible in this response region. Overall, in this region of parameter space, the trends are well behaved.

For  $f_e/f_n > 0.8$  the trend of various force curves distinct. For  $f_e/f_n = 0.85$ , the  $C_{D,mean}$  value increases for all amplitudes considered. For  $f_e/f_n = 0.9$ , the  $C_{D,mean}$  values increase up to  $A^* \leq 0.4$ . At higher amplitudes the  $C_{D,mean}$  values are reduced. However, the  $C_{D,rms}$  values show an increase at all amplitudes. In this region,  $C_{L,mean}$  is nonzero due to the asymmetrical nature of the P mode vortex shedding. For  $A^* > 0.4$ , the values of the mean and RMS lift coefficient are considerably less than the values found at lower amplitudes. The vortex-shedding mode resembles the S-II vortex-shedding mode. The S-II mode has zero mean and RMS values in the lift coefficient. In the present case, since the flow is not completely in the S-II

vortex-shedding mode, only a reduction in the mean and RMS values is observed. The considerable nonzero mean value of the lift coefficient is found only around the region in the parameter space  $0.85 \leq f_e/f_n \leq 1.1$ . The  $C_{L,mean}$  can be either positive or negative depending on the direction of vortex shedding. For  $f_e/f_n = 1.1$ , a considerable mean lift coefficient is observed only above  $A^* > 0.4$ . For  $f_e/f_n > 1.1$ , the  $C_{D,mean}$  value increases with an increase in the driving frequency ratio, while the trend in the case of the  $C_{D,rms}$  value is mixed. In general, an increase in  $A^*$  for a given  $f_e/f_n$  increase the values of the force coefficients. The  $C_{L,rms}$  values increase with an increase in the amplitude for a given frequency ratio.  $C_{L,mean}$  becomes negligible in this region of parameter space once again. Cetiner and Rockwell (2001) observed an increase in the RMS value of the lift coefficient within the synchronization regions as well. As discussed previously, this is not only due to the increased strength of vortical regions but also due to the vortical region forming closer to the body.

### 3.3. Energy transfer between the fluid and bluff body

According to Williamson and Govardhan (2004), the total force acting on the body can be decomposed into the potential force and the vortex force. A change in the phase of the vortex force with respect to the inline excitation can indicate a change in the energy transfer between the fluid and the bluff body. The timing/phase of vortex shedding with respect to the excitation is an important parameter in both inline and transverse vibration and can determine the energy transfer between the fluid and the bluff body (Singh et al., 2009; Sewatkar et al., 2012). As seen from the previous discussion about various vortex-shedding modes, the relative phase at which the vortices form a pair changes, especially near the harmonic synchronization region. It is useful to check whether such a phase change entails any change in energy transfer.

To assess the effect of the change in the phase of the vortex shedding, the work done by the excitation force during a cycle of excitation can be calculated from the perspective of relative motion between the bluff body and the fluid. The fluid can be considered to be flowing at a mean velocity, while the bluff body is under a relative sinusoidal motion. Under such conditions, the timing of pulsation from (a)–(c), which is shown in Fig. 5, can be interpreted as the downstroke/co-flow stroke and (c)–(e) can be considered as the upstroke/counterflow stroke of the bluff body. The dimensionless energy transfer rate and the coefficient of energy transfer is defined below in order to characterize the energy transfer (Konstantinidis and Balabani, 2007)

$$C_E = \int_0^1 C'_D(t) \frac{\dot{x}_c(t)}{u_m} d\frac{t}{T_e} = \int_0^1 \dot{e} d\tau \quad (5)$$

where  $C'_D(t)$  is the fluctuating part of the drag signal is defined as  $C'_D(t) = C_D(t) - C_{D,mean}$ , and  $\dot{x}_c(t)$  is the relative velocity of the body with respect to the fluid, which is assumed to be moving at the mean velocity. In the case of inline pulsation,  $\dot{x}_c(t) = -u_f(t) \sin(2\pi f_e t)$ ;  $u_f$  is the fluctuating velocity; and  $f_e$  is the frequency of the inline pulsation. Eq. (5) can also be interpreted as when drag increases during the downstroke and decreases during the upstroke, there is positive energy transfer between the body and fluid. The mean drag does not affect the energy transfer according to Eq. (5) because the mean drag will only change the mean position at which the bluff body will undergo vibration when supported by a spring. When  $C_E$  is positive, the fluid excites the vibration and damps it when the sign is opposite. This quantity depends on the near-body vortical events and is, hence, expected to strongly correlate with the vortex-shedding mode. For example, the P+S mode is associated with negative damping and is, hence, not expected to be present in in-line free vibration experiments.

To the best of authors' knowledge, it is not known whether the 2P + 2S mode and the modulated wake or the P mode is present in in-line free vibration experiments. However, the symmetric mode (S-I mode) is known to occur in inline free vibration (Konstantinidis and Balabani, 2007; Jauvits and Williamson, 2004). Note that several authors find a symmetric mode at  $f_e/f_n = 3.0$  and at much lower amplitudes when compared ( $\sim 0.3$ ) to the present case. At sufficiently high amplitude, the inline excitation imposes itself and causes a symmetric vortex-shedding mode. However, the amplitude at which the symmetric mode appears depends on the frequency.

The rate of energy transfer for all observed vortex-shedding modes along with the timing sinusoidal pulsation is plotted in Fig. 16. The 2P + 2S mode shows negative energy transfer, as seen in Fig. 16. This is also evident from the timing of the plots, given in Fig. 16(a). This is due to the shedding of the pair of vortices in the latter part of the cycle. The modulated wake also shows a similar trend. In this case, it is most likely due to the negative energy transfer that is associated with the normal antisymmetric vortex-shedding mode. However, in the P mode, the energy transfer is positive. This positive energy transfer is associated with the formation a pair of vortices at an earlier part of the inline excitation. As expected, the symmetric mode transfers energy from the fluid to the bluff body. In addition, it is found that the P mode is also associated with the same. The rate of energy transfer for various vortex-shedding modes is given in Fig. 16. The figure covers all the vortex-shedding modes that are observed in the present study. In Fig. 17, the relative timing of the symmetric mode that is given by Konstantinidis and Balabani (2007) is compared with the symmetric mode observed for a square cylinder. The timing of the various stages of vortex shedding is nearly the same, as can be observed in Fig. 17, which further confirms a positive transfer of energy.

## 4. Discussion

For the natural vortex shedding mode, the spectral content of lift coefficient correlates with the vortex shedding frequency and the drag frequency is twice the natural vortex shedding frequency. The empirical expressions such as Morison's equation, which are used for calculating loads acting in a purely oscillatory flow it is implicitly assumed that

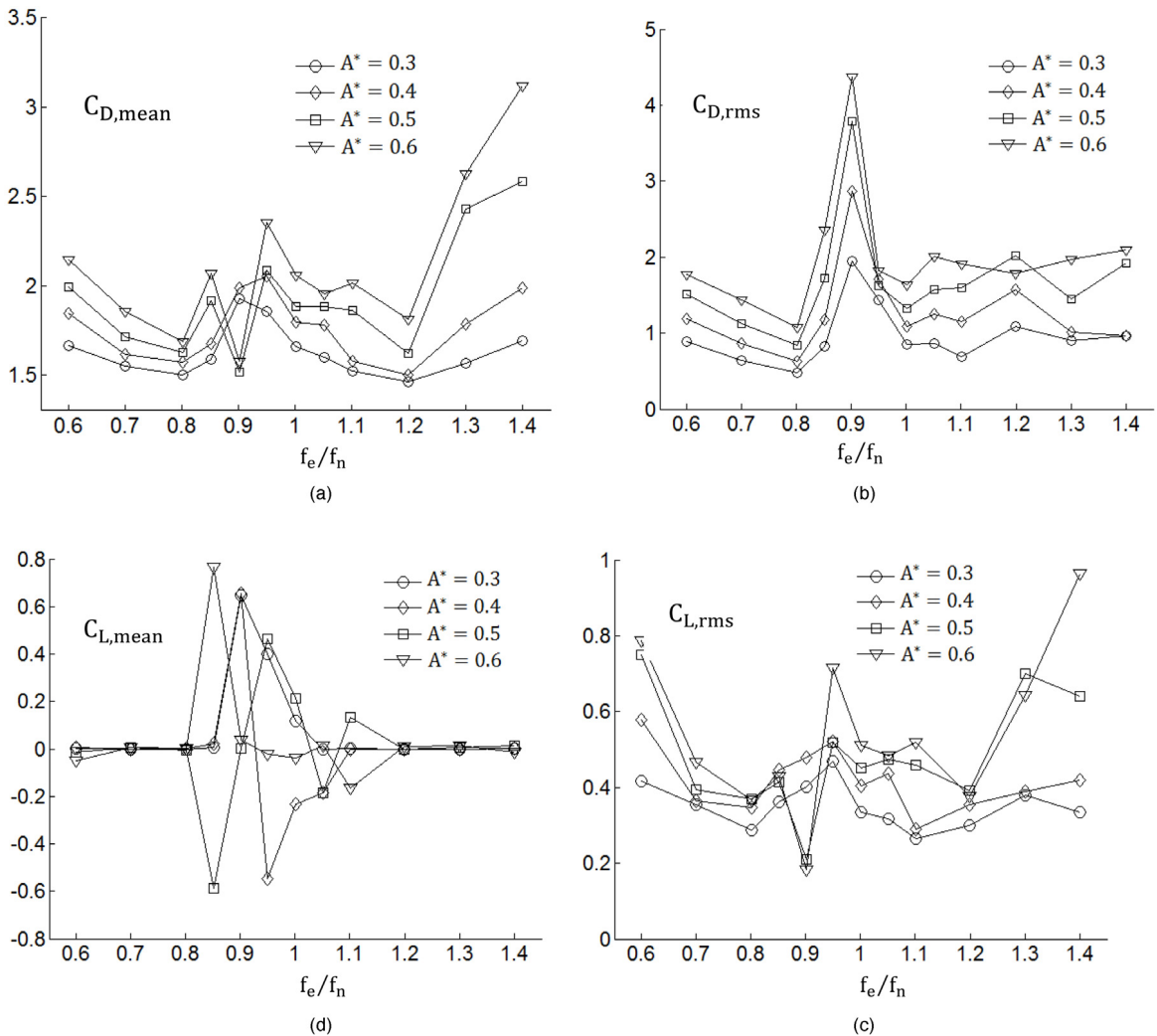


**Fig. 15.** Mean and rms force coefficients versus driving frequency ratio for various amplitudes (a)  $C_{D,mean}$  vs.  $f_e/f_n$  (b)  $C_{D,rms}$  vs.  $f_e/f_n$  (c)  $C_{L,mean}$  vs.  $f_e/f_n$  (d)  $C_{L,rms}$  vs.  $f_e/f_n$ .

the inline force coefficient has the same frequency as the imposed excitation. For forced vortex shedding modes, under inline pulsatile flow with a mean component, the data available in literature correlating the vortical events with the force coefficients are sparse and need to be examined. In the present study, we correlate the near body vortical events with the corresponding force coefficients, for the forced vortex shedding modes of a square cylinder subjected to inline pulsatile flow. In general, it can be expected that the stronger vortical structures which evolve nearer to the body, will leave a stronger trail on the force coefficients according to Eq. (1). The present study indicates that not all the vortical events are reflected in the force coefficients, the formation of which is not nearer to the bluff body. The slower frequency observed in the lift spectra for modulated wake is correlated to the swinging of the wake observed, however, the higher frequency content could not be correlated to the vortical phenomenon. During the pair formation process, in both  $2P + 2S$  mode and  $P$  mode, an upward pair shedding is strongly correlated with a downward mean lift coefficient and vice versa. The  $P$  mode is characterized by the distinct zero-frequency component in the spectra which is due to the pair formation above/below the wake centerline consistently over a large number of cycles, creating a mean lift. For  $2P + 2S$  mode, pair formation direction alternates, in alternate cycles and hence lift coefficient is mirror symmetric with no mean lift. The major frequency content of the drag coefficient is always same as the imposed excitation. As a thumb rule, the mean drag, RMS drag values increase with increasing amplitude of the pulsation through the entire region, although exceptions are possible. For example, for symmetric vortex shedding mode, the mean drag reduces while RMS drag value increase with amplitude compared to lower amplitude antisymmetric modes. Within the synchronization region, the RMS values of the lift and drag coefficients are higher when compared to the nonsynchronization regions, except when the symmetric mode occurs. Similar observations

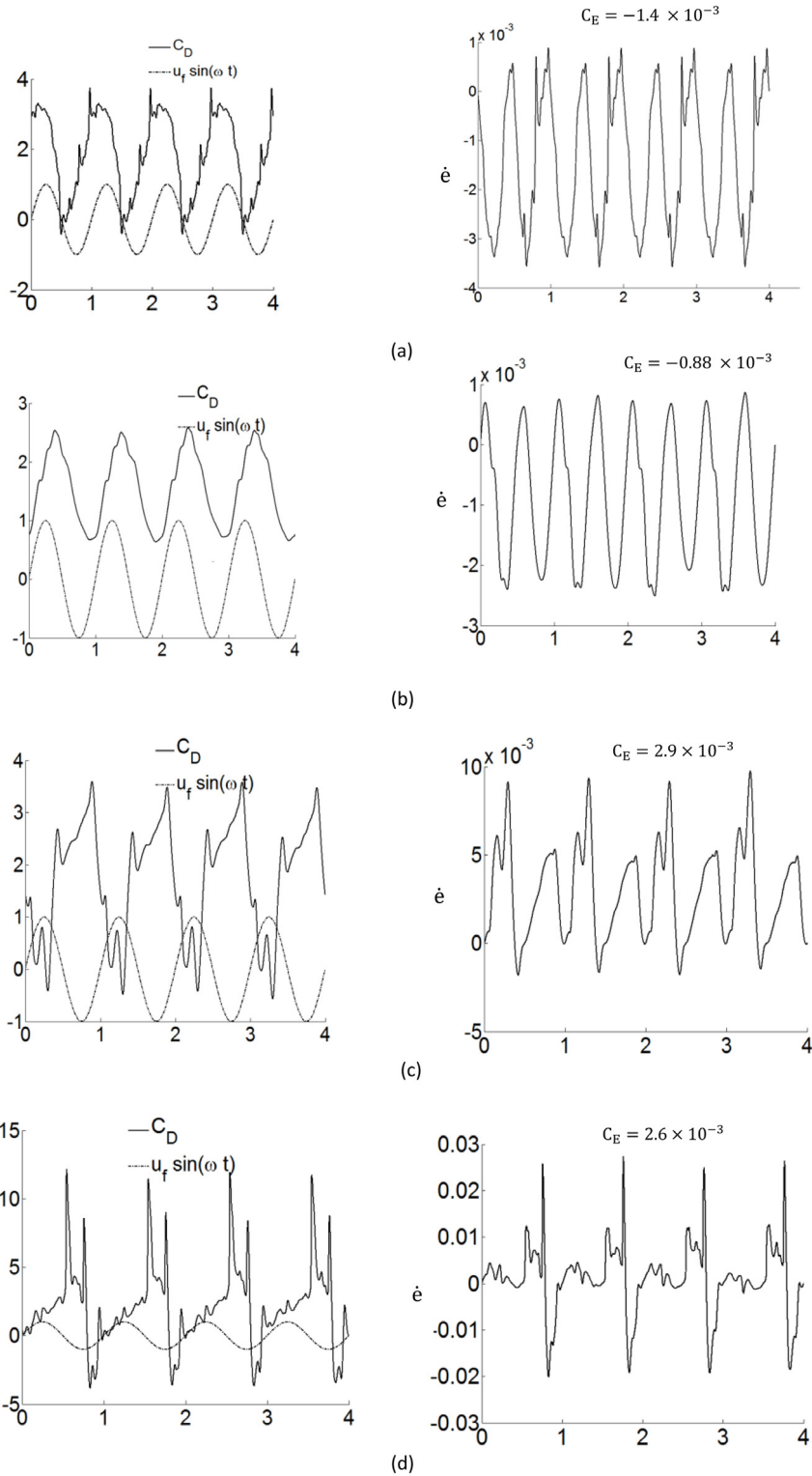


**Fig. 16.** For four time-period of external pulsation ( $4T_e$ ), temporal variation of drag coefficient and corresponding energy exchange at  $Re = 100$ , (a)  $f_e/f_n = 0.6$ ,  $A^* = 0.4$ :  $2P + 2S$  mode; (b)  $f_e/f_n = 0.8$ ,  $A^* = 0.4$ : Modulated wake mode; (c)  $f_e/f_n = 1.0$ ,  $A^* = 0.4$ : P mode; and (d)  $f_e/f_n = 0.9$ ,  $A^* = 0.5$ : symmetric mode.

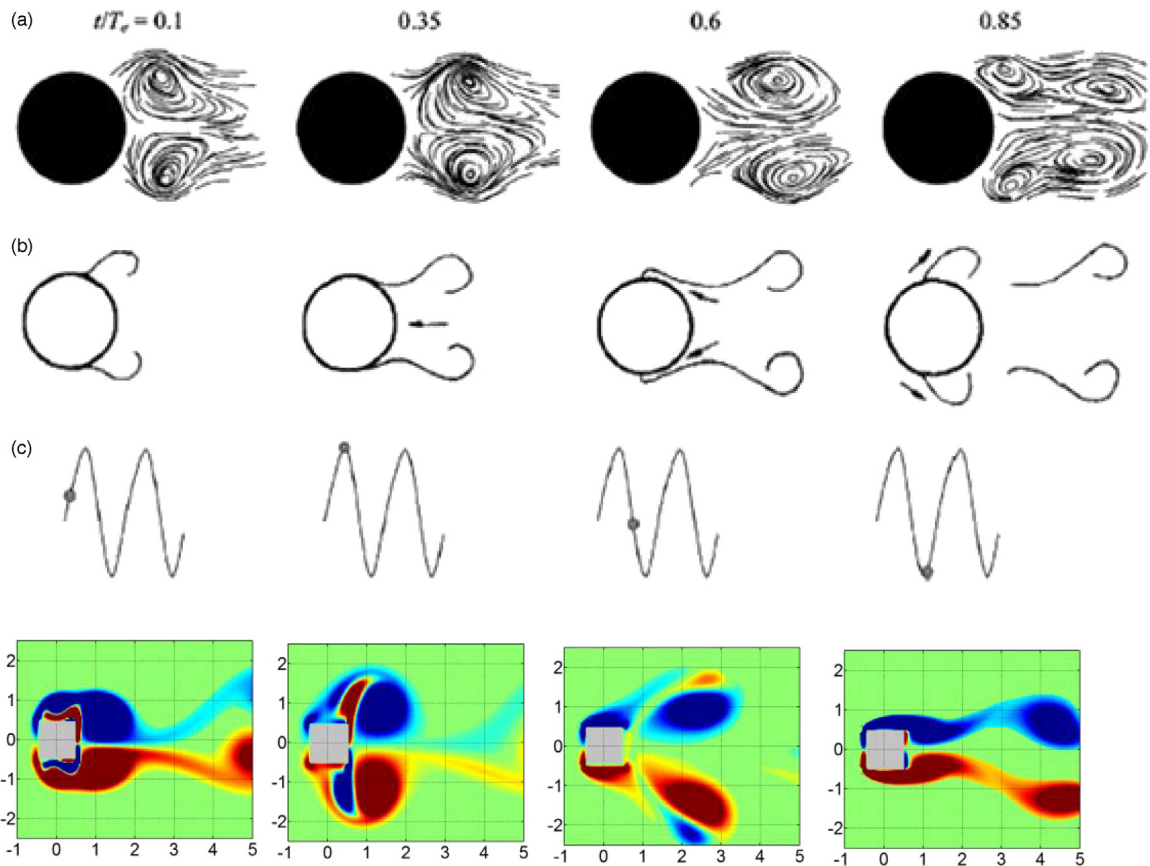


**Fig. 17.** Comparison of the timing of vortex shedding with respect to inline pulsation, taken from [Konstantinidis and Balabani \(2007\)](#) for a circular cylinder, and current results for a square cylinder.

have been made by [Cetiner and Rockwell \(2001\)](#). This can be attributed to the formation of vortical structures nearer to the body, as is evidenced from the positions of various vorticity maxima nearer to the body, especially in the synchronization region.

The effect near body vortical events on the energy transfer between fluid and bluff body is also examined in detail for forced vortex shedding modes observed in the study. It is observed that the timing of vortex pair formation strongly influences the energy transfer between the fluid and bluff body for both 2P + 2S mode as well as P mode. Based on the change in the nature of for energy transfer coefficient observed in the present study, it can be inferred that the pair vortical formation during the downstroke likely promotes flow-induced motion of the bluff body, while the pair of the vortical formation during the upstroke damps the flow-induced motion of the bluff body. The difference in the timing of pair formation of vortex pair implies that while for P mode there is significant positive energy transfer between the fluid and bluff body, for the 2P + 2S mode the energy is negative. [Singh et al. \(2013\)](#) observed that the 2P mode causes a damping from the fluid and, hence, cannot be observed in free inline vibration experiments. The dynamics of the formation of the 2P mode, which was presented by [Singh et al. \(2013\)](#), resembles the 2P + 2S mode that is presented here, without the formation of the S mode. From the presented results, it can be inferred that the pair of formations in the 2P mode should be at the end of the cycle that is similar to the 2P + 2S mode. Though this observation does not refute the possibility of occurrence of 2P mode under inline vibration experiments at a different parameter range, it can be expected that the timing of pair formation with respect to the inline excitation is different when compared to the 2P + 2S mode.

Information regarding the timing of the formation of the vortex and its correlation with the lift and drag coefficients are not only useful in ascertaining of the energy transfer between the bluff body and fluid but also in the understanding the history of vortical structures that occur under bimodal vortex shedding, such as those observed by [Konstantinidis et al. \(2007\)](#) or when mode competition occurs within a cycle, as observed by [Cetiner and Rockwell \(2001\)](#) where instantaneous snapshots may not reveal the full history of the vortex shedding. The results presented here, in understanding the relative timing of formation of a pair of vortices can also be helpful in flow control strategies such as the VIV suppression using synthetic jets, to time the pulsation of the jets.

## 5. Conclusions

In the present study, we investigated the correlation of force coefficients with the near body vortical events of a square cylinder subjected to inline pulsatile flow, using Lattice Boltzmann Method. The investigation region consisted of moderate nondimensional amplitudes of pulsation up to 0.6 and frequency ratio ranging from 0.6 to 1.4 for a fixed  $Re = 100$ . Four canonical vortex shedding modes which were previously described for circular cylinder under different types of excitation were observed for the square cylinder. A subharmonic region with the  $2P + 2S$  mode, around frequency ratio 0.6 and harmonic region with mainly P mode was found. Towards the left boundary of the synchronization region, a symmetric mode was found at relatively lower amplitude. Outside these regions, a modulated wake was observed.

The frequency content of the spectra was correlated with the near body vortical events. It can be concluded that all vortical events need not be reflected in the spectra of force coefficients. For  $2P + 2S$  mode, both the lift and drag signal was dominated by the pair vortex shedding event. For modulated wake, the slower frequency content in the lift spectra was correlated with the swinging of the wake. For P mode, a mean lift was generated due to the persistent pair formation above the wake centerline. The trend for lift and drag, when a vortex pair formation occurs is similar for  $2P + 2S$  mode, however the direction of pair formation alternates in each cycle hence no mean lift is observed. The mean lift is responsible for the peak observed at zero frequency, for the P mode. The force coefficients show distinct trends in different regions of parameter space. Towards the left lock in the boundary of the harmonic region, the nature of fluid forces shows a drastic change, especially for the symmetric mode. The mean and RMS lift is reduced and the spectra of lift are broadband implying that no information regarding the vortical events is available in the lift coefficient. A closer inspection at the vorticity snapshots of different modes shows that stronger vortical formation, closer to the bluff body, in the harmonic synchronization region is responsible for the distinct behavior within that region. The analysis conducted in the present study suggests that  $2P + 2S$  mode is unlikely to be found in free inline vibration experiments around frequency ratio 0.6. A study on the relative timing of the vortical pair formation shows that for  $2P + 2S$  mode the vortical pair formation at the end of the cycle causes a damping from fluid while pair formation at the start of the cycle for P mode cause excitation from the fluid. This change in the nature of energy transfer as compared to P mode and the symmetric mode is attributed to the change in the timing of pair formation. It can be expected that a square cylinder may be prone to inline vibration around harmonic synchronization region at higher amplitudes. Though the exact numerical quantities are unlikely to be same across different bluff body shapes and at different Reynolds' number, the similarity in spectra and thereby its interpretation would still hold for vortex shedding modes observed under different conditions. It would be surprising if one were to find that the P mode or symmetric mode observed here, that will not cause a positive energy transfer for different bluff bodies for similar flow regimes. This inference is drawn purely from the relative timing of the vortical event with respect to the inline excitation.

The present results imply that for a drag coefficient for the inline pulsatile flow, which is always at the imposed frequency, irrespective of the vortex shedding mode, the use of an extended Morison's type of correlation proposed by several authors (see Zhou and Graham, 2000) to some extent, needs to be used with caution for inline pulsatile flow. The coefficients of such correlations are likely to vary significantly across different regions of the parameter space of the excitation. A detailed study of different correlations available in literature and its applicability to different regions, for different bluff bodies under various vortex shedding conditions needs to be investigated in a future work.

## References

- Al-Mdallal, Q.M., Lawrence, K.P., Kocabiyik, S., 2007. Forced streamwise oscillations of a circular cylinder: Locked-on modes and resulting fluid forces. *J. Fluids Struct.* 23, 681–701.
- Armstrong, B.J., Barnes, F.H., Grant, I., 1986. The effect of a perturbation on the flow over a cylinder. *Phys. Fluids* 29, 2095–2102.
- Barbi, C., Favier, D.P., Maresca, C.A., Telionis, D.P., 1986. Vortex shedding and lock-on of a circular cylinder in oscillatory flow. *J. Fluid Mech.* 170, 527–544.
- Bearman, P.W., Downie, M.J., Graham, M.R., Obasaju, E.D., 1985. Forces on cylinders in viscous oscillatory flow at low Keulegan–Carpenter numbers. *J. Fluid Mech.* 154, 337–356.
- Cetiner, O., Rockwell, D., 2001. Streamwise oscillations of a cylinder in a steady current. Part 1. Locked-on states of vortex formation and loading. *J. Fluid Mech.* 427, 1–28.
- Detemple-Laake, E., Eckelmann, H., 1989. Phenomenology of Karman vortex streets in oscillatory flow. *Exp. Fluids* 7, 217–227.
- Jauvits, N., Williamson, C.H.K., 2004. The effect of two degrees of freedom on vortex-induced vibration at low mass and damping. *J. Fluid Mech.* 509, 23–62.
- Konstantinidis, E., Balabani, S., 2007. Symmetric vortex shedding in the near wake of a circular cylinder due to streamwise perturbations. *J. Fluids Struct.* 23, 1047–1063.
- Konstantinidis, E., Balabani, S., Yianneskis, M., 2007. Bimodal vortex shedding in a perturbed cylinder wake. *Phys. Fluids* 19, 011701.
- Krishnan, H., Agrawal, A., Sharma, A., Sheridan, J., 2016. Near-body vorticity dynamics of a square cylinder subjected to an inline pulsatile free stream flow. *Phys. Fluids* 28, 093605.
- Kumar, S.R., Sharma, A., Agrawal, A., 2008. Simulation of flow around a row of square cylinders. *J. Fluid Mech.* 606, 369–392.
- Leontini, J.S., Jacono, D.L., Thompson, M.C., 2011. A numerical study of an inline oscillating cylinder in a free stream. *J. Fluid Mech.* 551–568.
- Leontini, J.S., Jacono, D.L., Thompson, M.C., 2013. Wake states and frequency selection of a streamwise oscillating cylinder. *J. Fluid Mech.* 730, 162–192.
- Ongoren, A., Rockwell, D., 1988. Flow structure from an oscillating cylinder Part 2. Mode competition in the near wake. *J. Fluid Mech.* 191, 225–245.
- Scolan, Y.M., Faltinsen, O.M., 1994. Numerical studies of separated flow from bodies with sharp corners by the vortex in cell method. *J. Fluids Struct.* 8, 201–230.
- Sewatkar, C.M., Sharma, A., Agrawal, A., 2012. On energy transfer in flow around a row of transversely oscillating square cylinders at low Reynolds number. *J. Fluids Struct.* 31, 1–17.
- Singh, S.P., Biswas, G., Nithiarasu, P., 2013. A numerical study of vortex shedding from a circular cylinder vibrating in the in-line direction. *Internat. J. Numer. Methods Heat Fluid Flow* 23, 1449–1462.

- Singh, A.P., De, A.K., Carpenter, V.K., Eswaran, V., Muralidhar, K., 2009. Flow past a transversely oscillating square cylinder in a free stream at low Reynolds numbers. *Internat. J. Numer. Methods Fluids* 61, 658–682.
- Smith, D.T., Leontini, J.S., Sheridan, J., Lo Jacono, D., 2012. Streamwise forced oscillations of circular and square cylinders. *Phys. Fluids* 24, 111703.
- Srikanth, T., Dixit, H.N., Rao, T., Govindarajan, R., 2011. Vortex shedding patterns, their competition, and chaos in flow past inline oscillating rectangular cylinders. *Phys. Fluids* 23, 073603.
- Succi, 2001. *The Lattice Boltzmann Equation for Fluid Dynamics and Beyond*, Oxford U.P.
- Tatsuno, M., Bearman, P.W., 1990. A visual study of the flow around an oscillating circular cylinder at low Keulegan–Carpenter numbers and low Stokes numbers. *J. Fluid Mech.* 211, 157–182.
- Williamson, C.H.K., 1985. Sinusoidal flow relative to circular cylinders. *J. Fluid Mech.* 155, 141–174.
- Williamson, C.H.K., Govardhan, R., 2004. Vortex-induced vibrations. *Annu. Rev. Fluid Mech.* 36, 413–455.
- Xu, S.J., Zhou, Y., Wang, M.H., 2006. A symmetric binary-vortex street behind a longitudinally oscillating cylinder. *J. Fluid Mech.* 556, 27.
- Zheng, W., Dalton, C., 1999. Numerical prediction of force on rectangular cylinders in the oscillating viscous flow. *J. Fluids Struct.* 13, 225–249.
- Zhou, C.Y., Graham, J.M.R., 2000. A numerical study of cylinders in waves and currents. *J. Fluids Struct.* 14, 403–428.